Oxidation of Metals, Vol. 63, Nos. 3/4, April 2005 (© 2005)
DOI: 10.1007/s11085-004-3198-z

Air Oxidation of FeCoNi-Base Equi-Molar Alloys at 800–1000°C

W. Kai,* W. L. Jang,* R. T. Huang,† C. C. Lee,* H. H. Hsieh,* and C. F. Du*

Received June 24, 2004; revised December 16, 2004

The oxidation behavior of FeCoNi, FeCoNiCr, and FeCoNiCrCu equi-molar alloys was studied over the temperature range 800–1000 °C in dry air. The ternary and quaternary alloys were single-phase, while the quinary alloy was two-phase. In general, the oxidation kinetics of the ternary and quinary alloys followed the two-stage parabolic rate law, with rate constants generally increasing with temperature. Conversely, three-stage parabolic kinetics were observed for the quaternary alloy at $T \geq 900°C$. The additions of Cr and Cu enhanced the oxidation resistance to a certain extent. The scales formed on all the alloys were triplex and strongly dependent on the alloy composition. In particular, on the ternary alloy, they consist of an outer-layer of CoO, an intermediate layer of Fe_3O_4, and an inner-layer of $CoNiO_2$ and Fe_3O_4. Internal oxidation with formation of FeO precipitates was also observed for this alloy, which had a thickness increasing with temperature. The scales formed on the quaternary alloy consisted of an outer layer of Fe_3O_4 and $CoCr_2O_4$, an intermediate layer of $FeCr_2O_4$ and $NiCr_2O_4$, and an inner layer of Cr_2O_3. Finally, the scales formed on the quinary alloy are all heterophasic, consisting of an outer layer of CuO, an intermediate-layer of CuO and Fe_3O_4, and an inner-layer of Fe_3O_4, $FeCr_2O_4$, and $CuCrO_2$. The formation of Cr_2O_3 on the quaternary alloy and possibly that of $CuCrO_2$ on the quinary alloy was responsible for the reduction of the oxidation rates as compared to the ternary alloy.

KEY WORDS: Oxidation; equi-molar alloys; Fe–Ni–Co–Cu–Cr.

*Institute of Materials Engineering, National Taiwan Ocean University, Keelung, 20224, Taiwan, Republic of China.
†Department of System Engineering and Science, National Tsing-Hua University, HsinChu, 30013, Taiwan, Republic of China.

INTRODUCTION

During recent decades, the high-temperature oxidation on structural materials, such as Fe-, Co-, and Ni-base alloys, has been investigated intensively and the results summarized in many reports.[1–3] In general, these alloys, developed for good oxidation resistance by adding adequate amounts of Al, Cr, and Si, are classified as alumina, chromia, and silica formers, depending on which oxide formed after achieving steady-state conditions. These oxides grow at an extremely slow rate on the alloy surface, acting as protective barriers against further reaction between the substrate and oxygen.[4,5] As a result, these alloys were extensively used for various applications in high-temperature, oxidizing environments.

Most recently, novel multicomponent alloys containing equivalent amounts of each alloying-element, so called equi-molar alloys (EMAs), were proposed. Generally speaking, EMAs contain the same atomic percentage of all the alloying elements, which offer a maximum-entropy value of the entire solid-solution and provide more thermodynamic freedom in the equilibrium state allowing the alloying design to achieve the material's stability for practical applications. In particular, EMAs can also be considered for use as structural materials with nano-grain crystalline or amorphous structures, having high strength and stiffness as well as excellent chemical properties.[6,7] In addition, the design of an alloy system with equi-molar compositions might provide an entirely different approach with respect to the traditional alloys based on a single principal element.

In order to develop EMAs which combine good corrosion resistance with better mechanical properties, several researches concentrated on FeCoNi-base EMAs are currently being undertaken in our laboratory. In view of this, it is of interest to initially investigate the oxidation behavior of three different EMAs in dry air, and particularly the roles of Cr and Cu additions on the oxidation kinetics of the FeCoNi ternary alloy.

EXPERIMENTAL

The starting materials of the alloys were small pieces of pure metals ($> 99.99\%$). Three EMAs, FeCoNi, FeCoNiCr, and FeCoNiCrCu containing equal amounts of each alloying element, were fabricated into 150-g button ingots by arc melting in a titanium-gettered argon atmosphere. All buttons were flipped over and remelted six times to ensure alloy homogeneity, and the test samples were directly sheared from the as-cast buttons. Detailed sample preparation procedures were described elsewhere.[8] The average weight and surface area of the specimens were 0.125 g and 1.6 cm^2, respectively.

The oxidation tests were performed by means of thermogravimetric analyzer (TGA, SETARAM TG 92-16) in dry air (>99.999% pure). For each experiment, the net flow rate of the air was kept constant at $40\,cm^3\,min^{-1}$, and the heating and cooling rates of the TGA furnace were set at $10°C\,min^{-1}$.

The microstructure of the as-cast alloys and oxidized samples was examined by X-ray diffraction (XRD) using monochromatic Cu–Kα radiation, optical microscopy (OM), scanning-electron microscopy (SEM) with energy-dispersive X-ray spectrometry (EDS), electron-probe microanalysis (EPMA) with X-ray wavelength-dispersive spectrometry (WDS). Extensive XRD analyses were performed on the scales, adopting a sequential grinding technique to study the spatial distribution of the various phases within the scales. XRD peaks were compared with JCPDS standard files to identify the various phases present. Some cross-sectional scales were further studied by transmission-electron microscopy (TEM equipped with EDS and selected-area diffraction (SAD)); the sample preparation was also described elsewhere.[9]

Some as-cast samples were etched with a nitric acid/hydrochloric acid solution for optical microscopy, and all the oxidized samples were unetched for SEM and EMPA examinations. Platinum wire (30 μm diameter) was used as a marker by spot-welding on the cleaned surface of the samples. The marker samples were oxidized and then prepared for microstructure examination by the same procedures described above.

RESULTS

Alloy Constitution

Figure 1 shows the microstructure of the three as-cast EMAs, showing that the ternary and quaternary EMAs were single-phase. Conversely, the quinary EMA revealed two different back-scattered-electron images (BEI) under SEM observation, consisting mostly of a gray dendritic-arm structure high in Co but low in Cu and of a light interface between the dendritic arms with a significantly high content of Cu (Cu-rich). Detailed EDS analyses of the composition of the three EMAs are reported in Table I.

Kinetics

Parabolic plots of the oxidation kinetics of the three EMAs over the temperature range 800–1000°C are shown in Fig. 2. In general, the oxidation kinetics of the ternary and quinary EMAs followed the two-stage

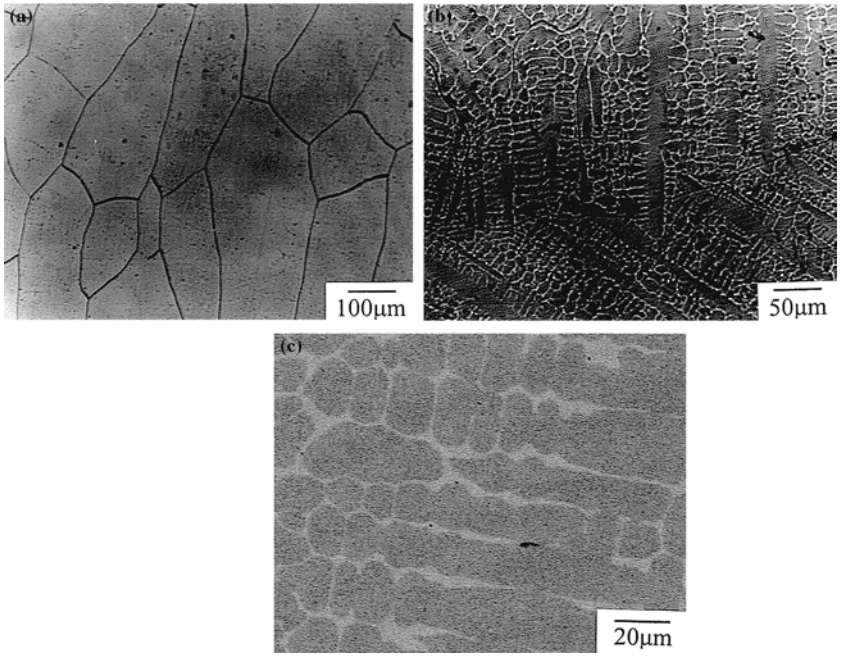

Fig. 1. Optical micrographs of (a) FeCoNi, (b) FeCoNiCr, and (c) BEI micrograph of FeCoNiCrCu.

Table I. EDS Analyses of the Compositions of FeCoNi-Base Equi-Molar Alloys.

(Elements) (Alloy/phase)	Fe	Co	Ni	Cr	Cu
FeCoNi	30.99	33.68	35.33	–	–
FeCoNiCr	25.06	24.77	24.32	25.85	–
FeCoNiCrCu (overall)	19.21	21.49	22.36	17.45	18.39
(bright phase)	0.90	1.08	11.60	4.24	82.18
(gray phase)	21.80	24.45	22.73	19.34	11.68

*These analyses were done in the areas shown in Fig. 1.

parabolic rate law, consisting of a fast initial, transient-state stage, followed by a slow, steady-state stage. Conversely, the oxidation kinetics of the quaternary EMA are much more complex and temperature-dependent, following a single-stage parabolic rate law at 800°C and a two-stage parabolic rate law at 850°C, while at least three-stage kinetics were observed at 900°C or higher, consisting of an initial, slow-growth transient oxidation, followed by a fast second stage, and then, by a third stage of intermediate rate. For example, the oxidation rate constant of

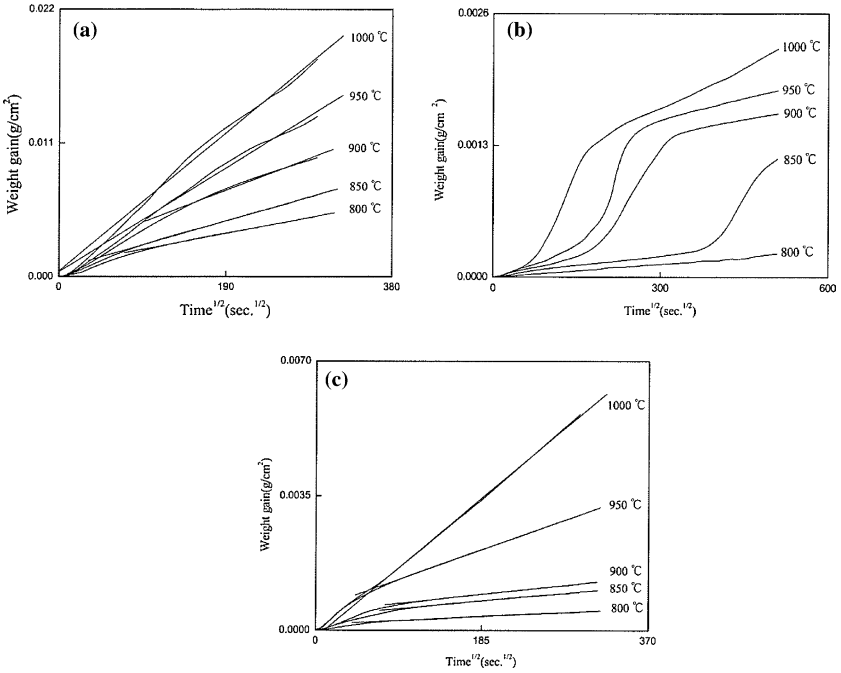

Fig. 2. Oxidation kinetics of the EMAs at 800–1000°C (a) FeCoNi, (b) FeCoNiCr, and (c) FeCoNiCrCu.

the quaternary EMA at 1000°C during the initial stage (up to $\sim$ 2.8 h) was approximately $4.08 \times 10^{-12}\,g^2\,cm^{-4}\,sec^{-1}$, after which it increased to $9.86 \times 10^{-11}\,g^2\,cm^{-4}\,sec^{-1}$ from 3 to 10 h, and then decreased down to $1.70 \times 10^{-11}\,g^2cm^{-4}sec^{-1}$ from 10 to 48 h. Similar oxidation kinetics was also observed at 900 and 950°C for the same alloy, although the duration at each kinetics stage gradually increased with decreasing temperature. The oxidation rate constants of the alloys are summarized in Table II, including the possible k_p's for various stages of the quaternary EMA. For comparative purposes, previous results for 316 stainless steel (316SS) tested in the same environments are also reported in Table II.[10] An Arrhenius plot of the oxidation rate constants is shown in Fig. 3; the corresponding activation energies are also given in Table II. As can be seen in Table II, the k_p values of the ternary EMA are much higher than those of the other alloys. For example, the k_p values of the ternary EMA are reduced by 3.07 orders of magnitude at 800°C, 2.16 orders of magnitude at 900°C, and 2.32 order of magnitudes at 1000°C by the addition of chromium (using the third-stage data). The addition of chromium and copper

Table II. Steady-State Oxidation Rate Constants ($g^2\,cm^{-4}\,sec^{-1}$) and Apparent Activation Energies (KJ/mole) of FeCoNi-Base Equi-Mnolar Alloys.

Compound	800°C	850°C	900°C	950°C	1000°C	Q(KJ/mol)
FeCoNi	2.31×10^{-10}	4.33×10^{-10}	1.02×10^{-9}	1.72×10^{-9}	3.60×10^{-9}	159.4
FeCoNiCr*	1.95×10^{-13}	(1)3.99×10^{-13}	(1)1.77×10^{-12}	(1)3.69×10^{-12}	(1)4.08×10^{-12}	–
		(2)6.40×10^{-11}	(2)3.09×10^{-11}	(2)2.29×10^{-11}	(2)9.86×10^{-11}	
			(3)6.92×10^{-12}	(3)5.66×10^{-12}	(3)1.70×10^{-11}	
FeCoNiCrCu	1.30×10^{-12}	4.67×10^{-12}	6.45×10^{-12}	6.99×10^{-11}	3.84×10^{-10}	316.5
316 SS	1.47×10^{-13}	–	1.10×10^{-11}	–	5.38×10^{-10}	397.6

*Note: The oxidation behavior of the quaternary EMA followed single-stage kinetics at 800°C, two-stage kinetics at 850°C, and three-stage kinetics at $T \geq 900\,°C$.

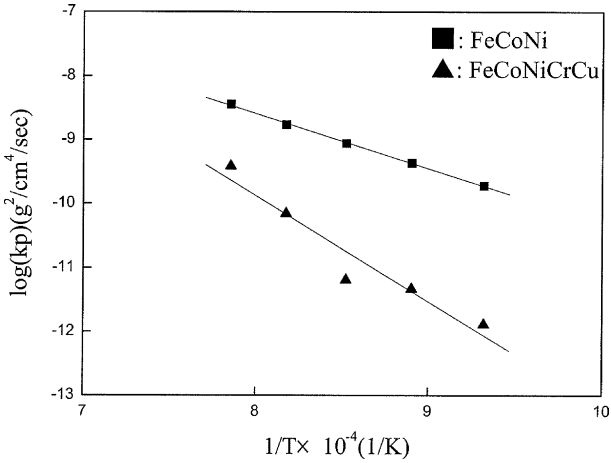

Fig. 3. Temperature dependence of the oxidation rate constants of FeCoNi-base EMAs.

to the quinary alloy reduces the k_p values by 0.97–2.24 orders of magnitude at 800–1000°C as compared to those of the ternary EMA. Furthermore, the k_p values of 316SS are much lower than those of the ternary EMA by 3 orders of magnitude at 800°C, 2 orders of magnitude at 900°C, and around 1 order of magnitude at 1000°C. In addition, the k_p values of the quaternary EMA are nearly identical to that of 316SS at 800°C, and slightly slower at 900–1000°C. Yet, the quinary alloy exhibited a faster oxidation rate at 800°C by 1 order of magnitude but also slightly slower rates at 900–1000°C (by factors of 1.4–1.7), as compared to those of 316SS.

Furthermore, the apparent activation energy of the ternary EMA ($159.4\,KJ\,mole^{-1}$) was much lower than those of 316SS ($\sim 400\,KJ\,mole^{-1}$) and the quinary EMA ($316.5\,KJ\,mole^{-1}$), implying that the oxidation mechanism of the EMAs is different and strongly composition-dependent.

On the contrary, the Q values of the quaternary EMA could not be obtained due to the complex kinetics, as indicated previously. The different between the k_p and Q values for the three EMAs are due presumably to the different nature of the scales formed on the various alloys, resulting in different principal species diffusing during oxidation, as will be discussed later.

Microstructure and Phase Constitution of Scales

Typical XRD analyses of the scales formed on the EMAs at 1000°C are shown in Fig. 4. The scales formed on the EMAs were complex and heterophasic, while their nature depended strongly on composition. The scales formed on the ternary EMA (Fig. 4a) consisted of an outer-layer of CoO, an intermediate-layer of Fe_3O_4 (cubic structure), and an inner-layer of $CoNiO_2$ and Fe_3O_4. In addition, the intermetallic Ni_3Fe phase was also detected on top of the substrate, revealing a Ni enrichment due to preferential oxidation of Co and Fe. However, XRD analyses failed to identify the internal-oxide particles of FeO that were observed by SEM analyses, as indicated in the following section. The scales formed on the quaternary EMA (Fig. 4b) consisted of an outer-layer of Fe_3O_4 and $CoCr_2O_4$, an intermediate-layer of $FeCr_2O_4$ and $NiCr_2O_4$, and an inner-layer of Cr_2O_3. Finally, the scales formed on the quinary EMA (Fig. 4c) were composed of an outer layer of CuO, an intermediate-layer of CuO and Fe_3O_4, and an inner-layer of Fe_3O_4, $FeCr_2O_4$ and $CuCrO_2$. In addition, it should be pointed out that XRD spectra to identify Fe_3O_4 produced an average of 0.2-degree shift (per 2θ) to higher angles, resulting in making a difficult distinction from Fe_2O_3 in the alloys, which can be solved by TEM analyses, as described later.

Since XRD results revealed the complexity of the scales formed on various EMAs, the scale morphology and phase constitution on the three EMAs will be described separately.

Ternary FeCoNi-EMA

Figure 5a shows the general surface morphology of the scales formed on the ternary EMA at 950°C for 24 h, revealing that large-facet CoO scales were formed. Typical cross-sectional BEI micrographs of the scales formed on the ternary EMA at various temperatures are shown in Fig. 5b–e. The scales were triplex and heterophasic, and remained well adherent to the substrate although numerous pores were noted. The porous outer-layer of CoO was very thin at 800°C (Fig. 5b) but became evident at $T \geq 900$°C (Fig. 5c–d). Although the boundary between the intermediate and inner layers was not so clear at $T \leq 900$°C, the formation of the triplex

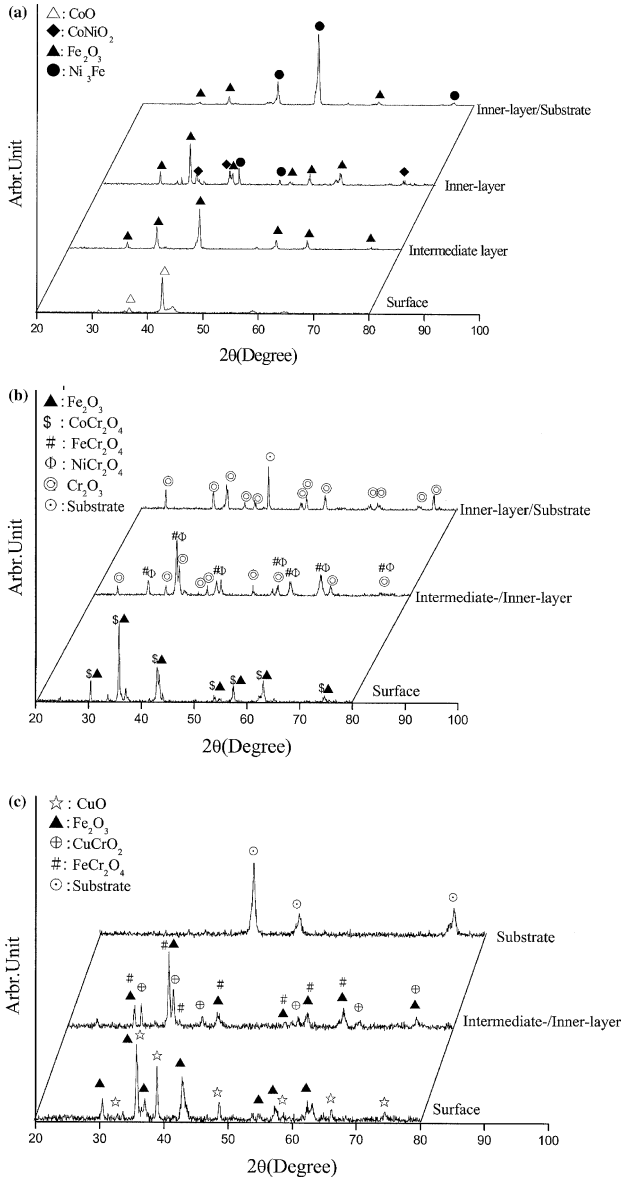

Fig. 4. XRD analyses of the scales formed at 1000°C after 24 h on (a) FeCoNi, (b) FeCoNiCr, (c) FeCoNiCrCu.

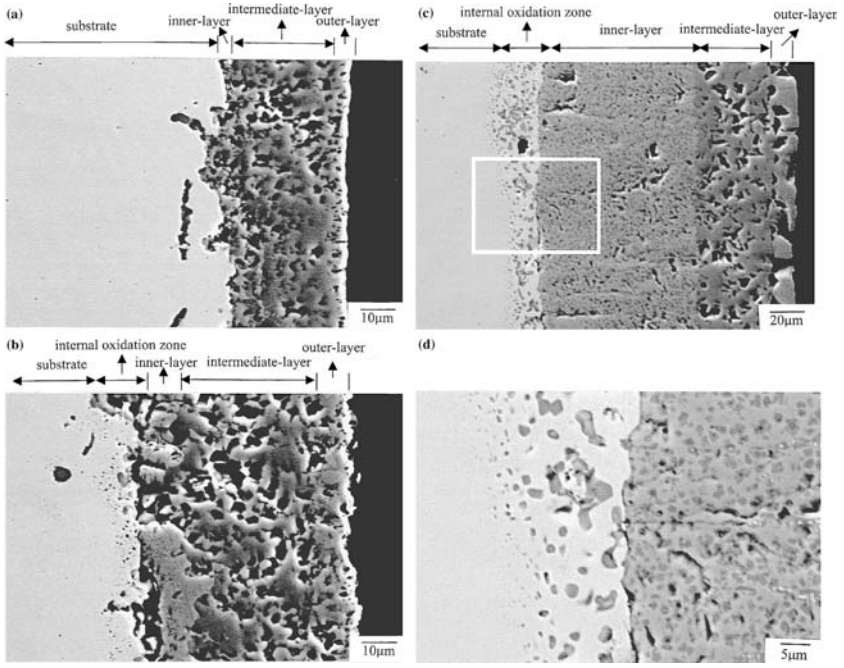

Fig. 5. Cross-sectional BEI micrographs of FeCoNi oxidized for 24 h (a) at 800°C, (b) at 900°C, (c) at 1000°C, and (d) high magnification of (c).

scales was confirmed by EPMA analyses. The thickness of the inner layer significantly increased with increasing temperature (with the same 24-h oxidation), while that of the intermediate layer remained nearly the same. At higher magnification (Fig. 5e), the inner layer revealed the presence of two different phases. The gray phase was rich in Co (26.36%, hereinafter at.% is used), Ni (23.78%), and O (49.51%), but low in Fe (0.35%), so that it corresponded to $CoNiO_2$. The analyses are in good agreement with XRD results mentioned above. On the contrary, the dark phase was rich in Fe (39.18%) and O (58.97%), but low in Ni (1.75%) and Co (0.20%). This composition may be close to Fe_2O_3 or Fe_3O_4 with dissolved Ni and Co, and thus, the EPMA analyses failed to distinguish the two iron oxides. Thus, to clarify the exact phase constitution of iron oxides, TEM analyses of the cross-sectional scales were prepared, and the results inserted with the SAD pattern are shown in Fig. 6. Based on the two SAD patterns

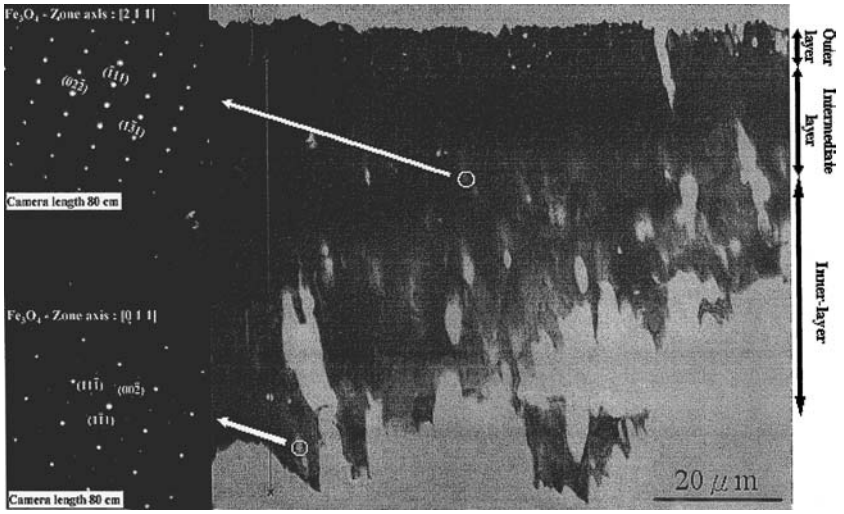

Fig. 6. TEM cross-section of the scales formed on FeCoNi oxidized for 24 h at 900°C and inserted SAD patterns of the local regions.

taken from the intermediate and inner layers, it is clearly that Fe_3O_4 was present in the two layers, while Fe_2O_3 was absent.

In addition, numerous sub-surface precipitates in the region below the alloy/scale interface were observed. The amount and size of the internal-oxide particles gradually increased with increasing temperature (from 800 to 900°C), while even an internal-oxide band (IOB) formed at 1000°C. The average composition of five different internal-oxide particles at 1000°C analyzed by WDS was 45.57% Fe, 6.73% Co, 6.47% Ni, and 41.23% O which is close to FeO with small amounts of non oxidized Co and Ni. A continuous layer of FeO is always present in the oxidation of pure Fe and Fe–Ni alloys above 570°C,[11] where FeO was thermodynamically stable. On the contrary, the internal FeO particles mixed with pure copper were observed in the oxidation of two-phase Fe–Cu alloys containing 25, 50, and 75 wt.% Cu under low oxygen pressures (10^{-11} Pa at 800°C and 10^{-8} Pa at 900°C)[12]. Thus, the presence of the internal FeO particles indicates that the oxidation mechanism of the ternary EMA is different from previous results in the literature, as will also be discussed later. Furthermore, the average composition of the light continuous phase within the IOB at 1000°C analyzed by WDS corresponded to a significantly high content of Ni (74.50%) and Fe (24.85%), but low of Co (0.65%) with no O, indicating that Ni enriched forming Ni_3Fe by a phase transformation.

Quaternary FeCoNiCr-EMA

Small network-shaped oxide particles formed on the surface of the scale on the quaternary EMA after oxidation at 1000°C for 72 h are shown in Fig. 7a. Cross-sections of the scales formed on the same alloy at various temperatures are shown in Fig. 7b–c, revealing their triplex nature, consisting of a porous outer layer, a porous intermediate layer, and a compact, nonplanar inner layer. The scales also remained in good adherence with the substrate, and no spallation was observed at any temperature. The average EDS composition from six different regions of the outer layer after exposure at 900°C for 72 h was high in O (49.87%) and Fe (27.24%) plus some Co (13.09%), and minor amounts of Cr (5.23%) and Ni (4.71%). This may correspond to the formation of Fe_3O_4 and $CoCr_2O_4$ (with some dissolved Ni) but disagrees with the XRD results in Fig. 4. However, due to the heterophasic nature of the heavily-porous intermediate layer, EDS and WDS results failed to identify the possible scale compositions present. Furthermore, EDS analysis of five various regions of the inner layer gave an average composition of 55.77% O and 42.45% Cr as well as minor amounts of 0.95% Fe, 0.50% Ni, and 0.33% Co, indicating that a dense, continuous layer of Cr_2O_3 did form, in agreement with XRD analyses. No evidence of any internal-oxide particles was found in this alloy by SEM and EPMA. In addition, EPMA line scans of the cross section of scales formed at 1000°C for 48 h, given in Fig. 7d, reveal that the porous outer layer had large contents of Co, Fe and O, the porous intermediate layer had large contents of Ni and O, while the inner layer was mostly composed of Cr and O.

Quinary FeCoNiCrCu-EMA

Unlike the scales formed on ternary and quaternary EMAs, nodular-shaped scales were observed for the quinary EMA at 800°C for 24 h (Fig. 8a). The corresponding cross-sectional scales, shown in Fig. 8b, consist of a thin, compact outer layer, a porous intermediate layer, and an inner layer where the Cu-rich phase was preferentially oxidized.

The nature of the scales formed on the quinary EMA after oxidation at 1000°C for 24 h is further exemplified in Fig. 9, showing a cross-sectional BEI micrograph and the X-ray maps of five alloying elements and O. The scales are composed of three layers. The thickness of the outer layer increased slightly but that of the intermediate layer scale was much larger, as compared to those at 800°C. The amounts of pores present in the intermediate layer progressively increased with increasing temperature. A thin, outer layer (labeled as A in Table III) mostly composed of CuO, formed on top of a porous intermediate layer (labeled as B) containing

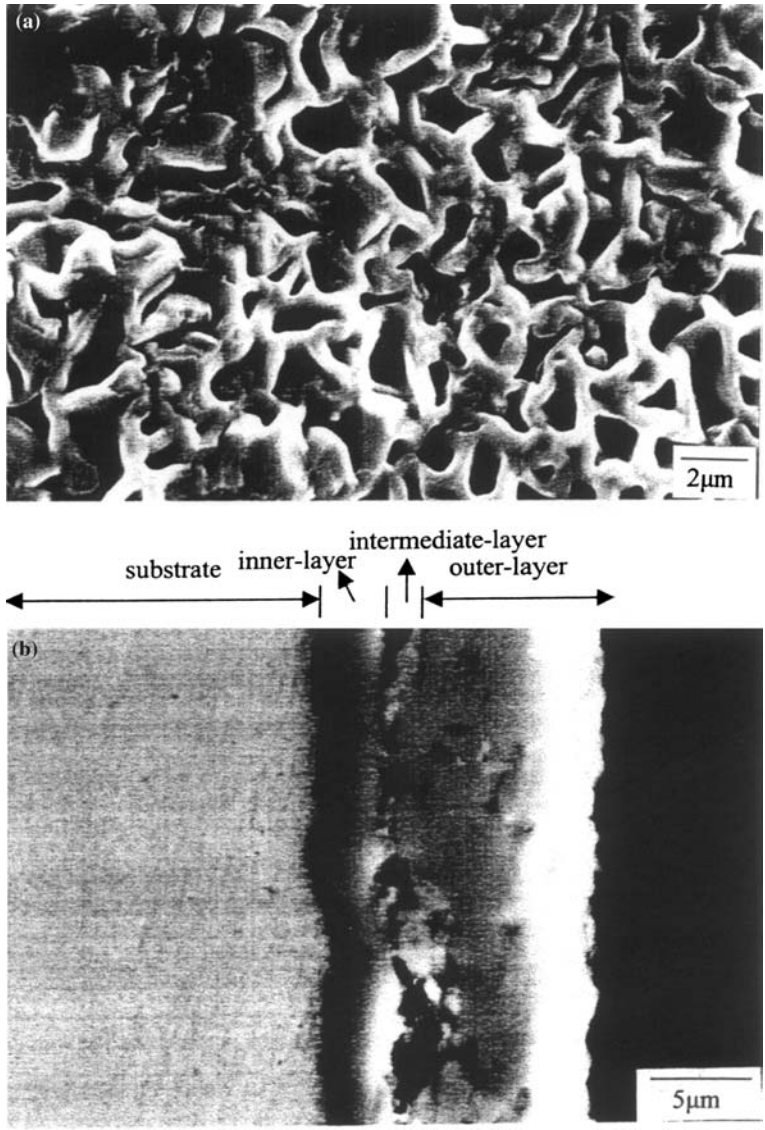

Fig. 7. (a) Surface micrograph of the scales formed on FeCoNiCr oxidized at 1000°C for 72 hr, and cross-sectional BEI micrographs of the same alloy oxidized at (b) 900°C for 72 hr, (c) 1000°C for 48 hr, and (d) EPMA traverses of (c).

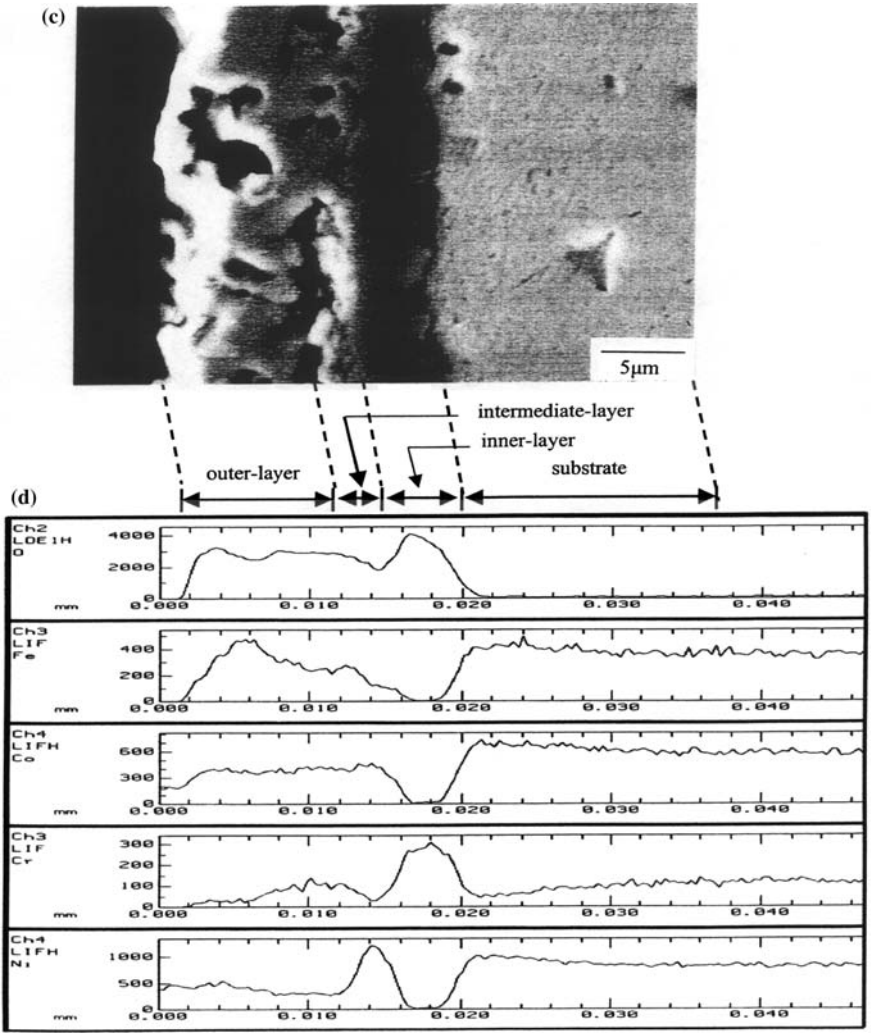

Fig. 7. Continued.

a mixture of CuO, Fe_3O_4, and $CuCrO_2$. The corresponding X-ray maps revealed the presence of significant amounts of Cu on top of the scales, while Fe, Cr, and Co concentrated mostly in the intermediate layer. In addition, the inner layer (labeled as C) along the dendritic interface had a large content of Cr (33.08%) and O (52.02%) plus some Fe (8.65%), and minor amounts of Cu (2.48%), Ni (1.90%), and Co (1.87%), while the dendritic phase (labeled as D) near the inner layer remained uncorroded

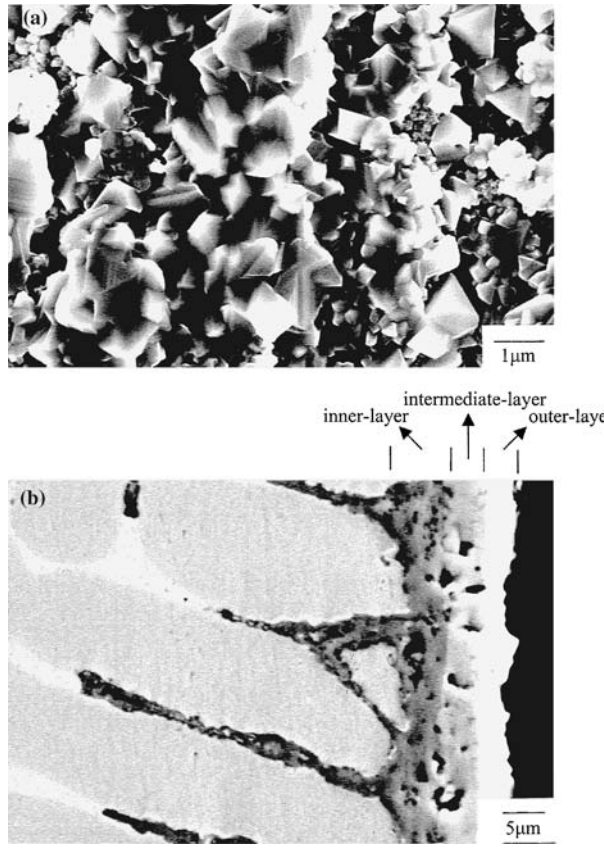

Fig. 8. (a) Surface micrograph of the scales formed on FeCoNiCr Cu at 800°C for 24 h and (b) cross-sectional BEI micrograph of (a).

and contained a large amount of Ni (32.58%) and Co (24.66%), but little Cu (2.85%) and no oxygen. On the other hand, the substrate far away from the inner layer (labeled as E and F) had a composition similar to the as-cast alloy as indicated in Table I.

Short-Term and Long-Time Oxidation

To clarify the initial oxidation behavior of the three EMAs, short-term oxidation tests were performed at 1000°C for various durations of time. Based on the SEM and XRD analyses, grayish nodule-shaped CoO mixed with white whisker-like particles were clearly observed in the ternary EMA after oxidation for 0.5 min (Fig. 10a). However, EDS failed to

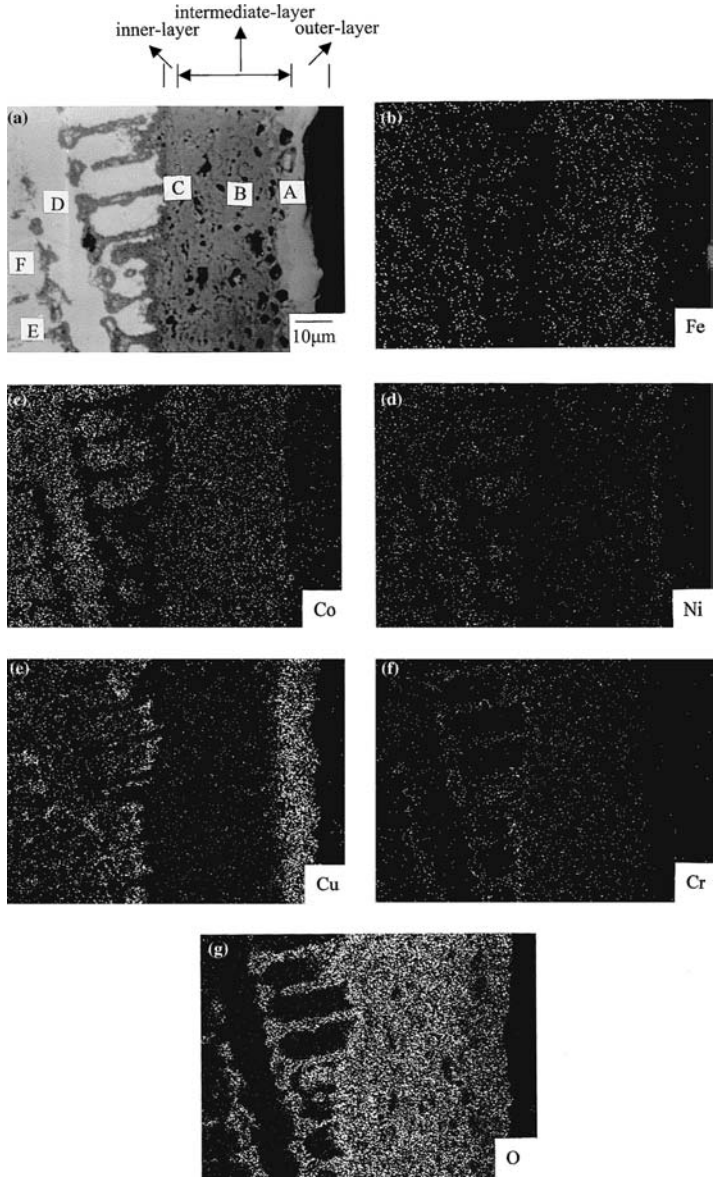

Fig. 9. (a) Cross-section BEI micrograph of FeCoNiCrCu oxidized for 24 h at 1000°C, and corresponding X-ray maps of (b) Fe, (c) Co, (d) Ni, (e) Cu, (f) Cr, (g) O of (a).

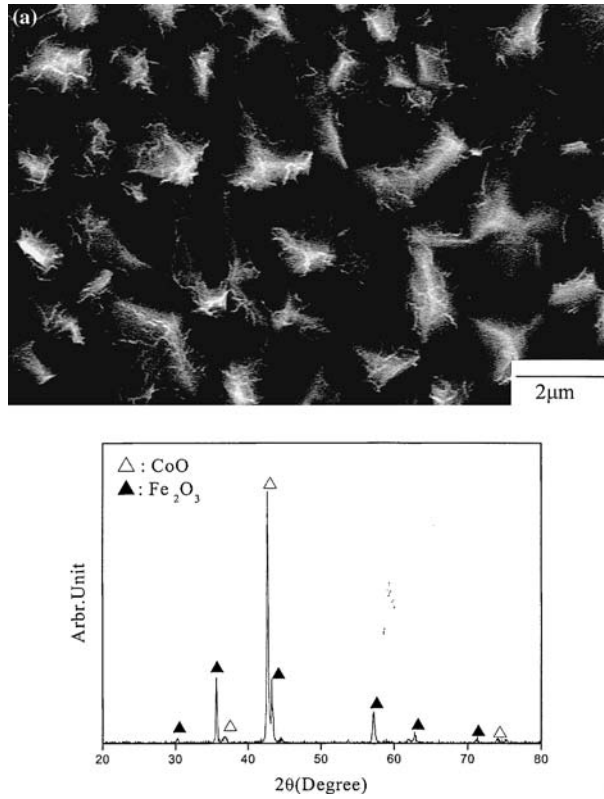

Fig. 10. Surface micrographs and XRD analyses of the scales formed on the EMAs oxidized at 1000°C (a) for 0.5 min in FeCoNi, (b) for 15 min in FeCoNiCr, and (c) for 2 min in FeCoNiCrCu.

Table III. EDS Analyses of the Scales in Fig. 9a

Position	Fe	Co	Ni	Cr	Cu	O
A	1.00	1.82	2.05	0.33	45.76	49.04
B	13.25	8.41	6.20	17.18	3.58	51.38
C	8.65	1.87	1.90	33.08	2.48	52.02
D	18.17	24.66	32.58	2.85	21.74	–
E	21.40	23.69	23.29	19.82	11.80	–
F	6.05	6.88	11.59	5.54	69.94	–

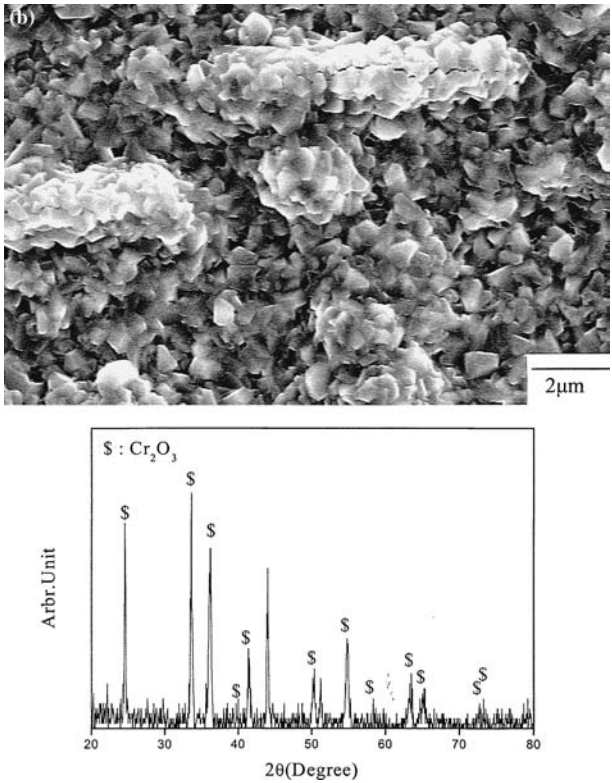

Fig. 10. Continued.

determine the exact composition since the whisker-like oxides are too thin to be examined. On the other hand, tiny granule-shaped Cr_2O_3 with dark-greenish color or small irregular grains of CuO with light-grayish color were observed for the quaternary (Fig. 10b) and quinary (Fig. 10c) EMAs, respectively.

Besides, some samples were also oxidized for long periods of time to study the final oxidation kinetics of the EMAs. A typical parabolic plot for the quaternary EMA oxidized at 1000°C for 240 h is shown in Fig. 11. Some corresponding BEI micrographs at various periods of time have also been inserted in the figure. A thin layer of Cr_2O_3 is observed at the initial stage, but some porous Fe_3O_4, $FeCr_2O_4$, $NiCr_2O_4$, and $CoCr_2O_4$ grow on top of the surface after 240-h exposure.

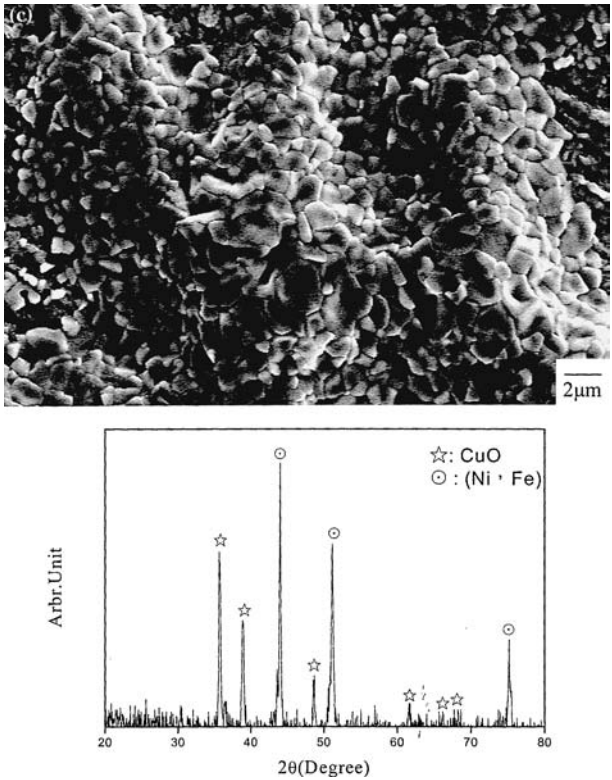

Fig. 10. Continued.

Marker Studies

Pt-marker studies were performed in order to investigate the oxidation mechanism of the EMAs. Typical BEI micrographs of the cross-section of the oxide scales formed on the ternary and quinary alloys at 1000°C for 24 h are shown in Fig. 12. The marker was always located at the interface between the inner scale layer and the substrate, indicating that the scale grew mainly by outward diffusion of cations.

DISCUSSION

The main goal of this research was to investigate the oxidation behavior of three different EMAs in dry air, and in particular to examine the effect of Cr and Cu additions on the oxidation kinetics. From the results described above, the important features of the oxidation behavior

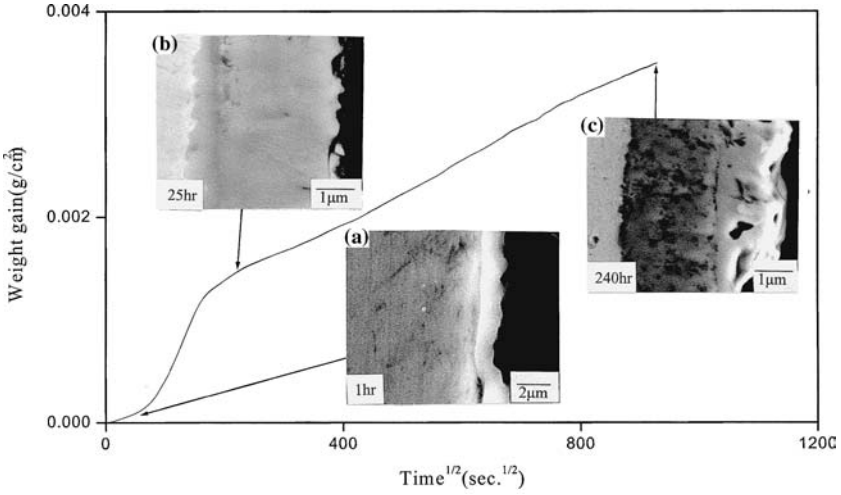

Fig. 11. Parabolic plots of long-time oxidation and the corresponding SEM micrographs of FeCoNiCr oxidized at various periods of time at 1000°C.

of EMAs in dry air can be summarized as follows: (1) oxidation followed the parabolic rate law, although two- or three-stage kinetics were noted; (2) for each alloy the oxidation rate constants increased with temperature; (3) the addition of Cr and Cu reduced the oxidation rates; (4) the scales formed on the alloys were heterophasic and complex, with a structure strongly depending on the alloy composition; (5) internal FeO particles and the formation of Ni_3Fe were observed for the ternary EMA; (6) during the initial stage of oxidation, mostly CoO with minor Fe_3O_4 formed on the ternary alloy, while Cr_2O_3 formed on the quaternary alloy and CuO on the quinary alloy; (7) the Pt marker was always located at the inner-layer/substrate boundary.

The oxidation kinetics of the three EMAs followed the parabolic rate law, although two- or three-stage kinetics were noted in the quaternary alloy, indicating that solid-state diffusion was the rate-limiting step throughout the oxidation reaction. The oxidation rate constants generally increased with increasing temperature due to a faster transport of reactants through the scales. Based on the results in Table II, the addition of both Cr in the quaternary alloy and Cr and Cu in the quinary alloy effectively reduced the oxidation rates at 800–1000°C as compared to those of the ternary alloy. However, in comparison with the quaternary alloy, the quinary EMA did not show a further reduction in the k_p values although the total amount of the alloying elements increased from 25% (exclusive Cr content) to 40% (Cr and Cu contents).

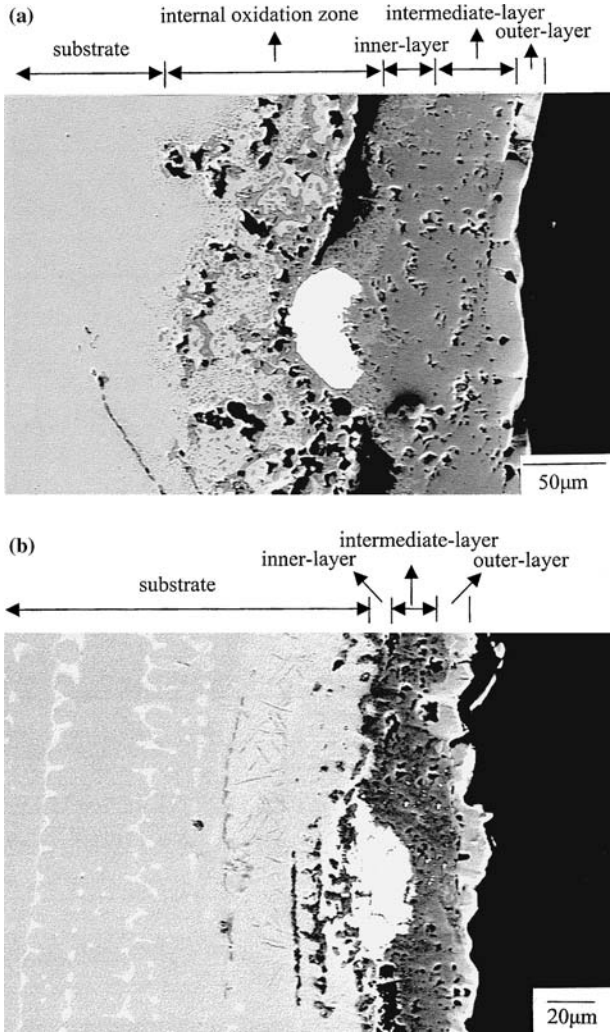

Fig. 12. BEI micrographs illustrating the position of Pt marker on the alloys oxidized at 1000°C for 24 h in (a) FeCoNi and (b) FeCoNiCrCu.

The oxidation of common metals (such as Fe, Co, and Ni) generally follows the parabolic rate law,[13–15] and the oxidation rate constants increased with increasing oxygen partial pressures, revealing that the principal scales are p-type semiconductors containing cation vacancies.

The scales formed on pure Fe at 1000°C are triplex, consisting of 95%FeO/4%Fe_3O_4/1%Fe_2O_3, while a single-layered NiO and a bi-layered CoO/Co_3O_4 form on pure Ni and Co, respectively. The non stoichiometry values (y) are around 0.05–0.12 for $Fe_{1-y}O$ at 1000°C, ~0.01 for $Co_{1-y}O$ at 1150°C, and $\sim 2.5 \times 10^{-4}$ for $Ni_{1-y}O$ at 1000°C, and self-diffusivities at 1000°C for Fe in FeO, Co in CoO, and Ni in NiO are around 1×10^{-7}, 1×10^{-9}, and 5×10^{-11} ($cm^2\,sec^{-1}$) in air or pure oxygen.[16–19] Thus, under a synergistic effect of highly defective nature of FeO and fast cation difusivity, the oxidation rate constant of pure Fe ($\sim 3 \times 10^{-7} g^2 cm^{-4}\,sec^{-1}$) is much higher than for pure Co ($\sim 3 \times 10^{-9}\,g^2\,cm^{-4}\,sec^{-1}$)and Ni ($\sim 9 \times 10^{-11} g^2\,cm^{-4}\,sec^{-1}$) at 1000°C.[11,13–15]

Based on XRD results, the scales formed on the three EMAs are triplex and strongly composition-dependent. As indicated before, the scales formed on the ternary EMA consist of an outer layer of CoO, an intermediate layer of Fe_3O_4, and an inner layer of $CoNiO_2$ and Fe_3O_4. Besides, according to the results of short-time oxidation, mostly CoO with minor amounts of Fe_3O_4 were observed, indicating that the outward diffusion of cobalt ions is much faster than that of iron, while nickel is the slowest-diffusing species. The reason for the formation of less-defective Fe_3O_4 but the absence of highly-defective, fast-growing FeO in the intermediate- and inner-layers is still unclear. Perhaps, some amount of FeO existed in the scale, but its amount was possibly too low to be detected, or it is possible that FeO formed internally rather than externally on the ternary EMA. As mentioned early, the formation of internal-oxide particles was always observed for two-phase Fe-base binary alloys,[12] but it is quite uncommon in the solid-solution alloys containing large amounts of Fe. Thus, it is worth discussing the formation of internal FeO particles in the current study.

According to the general criteria to form an internal oxide, [20] the growth of FeO particles is due to both thermodynamic and kinetic reasons. Based on the Gibbs free energies of formation per mole O_2,[21] FeO has the most negative value in the ternary EMA. Thus, the formation of internal FeO particles is certainly justified based on thermodynamics. The Fe content of the ternary EMA (around 33%) should be high enough for the formation of an external oxide layer. According to XRD/TEM results, a continuous, intermediate layer of Fe_3O_4 did form and some Fe_3O_4 also intermixed with $CoNiO_2$ in the inner layer. It is most likely that the formation of Fe_3O_4 results in a significant depletion of Fe in the alloy. Thus, the Fe concentration in the alloy near the scale may be insufficient to form a continuous oxide layer, thereby kinetically favoring the formation of internal FeO particles.

The oxidation of the quaternary EMA also produced triplex scales, consisting of an outer layer of Fe_3O_4 and $CoCr_2O_4$, an intermediate layer of $FeCr_2O_4$ and $NiCr_2O_4$ and an inner layer of Cr_2O_3. However, Cr_2O_3 always appeared during the first minute of oxidation, and formed even a continuous layer (in 1-h exposure in Fig. 11) before the appearance of other oxides, which corresponded to the initial, slow-growth kinetics in Fig. 2b. After a certain time of exposure (depending on temperature), Fe_3O_4, $CoCr_2O_4$, $FeCr_2O_4$, and $NiCr_2O_4$ formed on the scale surface. Very likely, the initial Cr_2O_3 layer is too thin to stop the transport of other cations. The formation of Cr_2O_3 during the initial stage of oxidation consumes Cr in the substrate, which in turn increases the activities of the other components (Co, Fe, and Ni), which can react with oxygen to form binary or ternary oxides, thereby resulting in the fast, second-stage kinetics, as also observed in Fig. 2b. After prolonged exposure (up to 240 h at 1000°C in the current study), the scaling rate reaches a third, steady-state kinetics stage, as shown in Fig. 10. Thus, a three-stage-kinetics behavior is observed for the quaternary EMA at higher temperatures ($T >$ 900 °C). The formation of Cr_2O_3 is responsible for the reduction of oxidation rates of the quaternary EMA, as compared to those of the ternary alloy. On the contrary, a single-stage or two-stage kinetics behavior was noted at 800 and 850°C, respectively. Perhaps, the dense Cr_2O_3 layer is sufficiently protective to completely suppress outward diffusion of other cations at 800°C, or the oxidation time is not long enough to reach the third steady-state at 850°C.

The oxidation behavior of the quinary EMA is somewhat different from the other two EMAs. First of all, this two-phase alloy oxidized to form heterophasic scales, consisting of an outer layer of CuO, an intermediate layer of CuO and Fe_3O_4, and an inner layer of Fe_3O_4, $FeCr_2O_4$, and $CuCrO_2$, while NiO was absent. Based on short-time oxidation, CuO always formed at the initial stage of oxidation, indicating that the Cu-rich phase was selectively oxidized. Secondly, the scales formed on pure Cu and Cu-base alloys at elevated temperatures are composed mostly of non-protective Cu_2O in the inner layer and minor amounts of CuO in the outer layer. However, Cu_2O was not observed in the current study. It is possible that Cu_2O has been completely consumed by reacting with Cr_2O_3 to form the ternary oxide $CuCrO_2$ by suppressing the growth of the non-protective Cu_2O. Although the defect structure of the ternary oxide is unknown, it is possibly less-defective than that of Cu_2O. Thus, the formation of $CuCrO_2$ is also beneficial for the reduction of oxidation rates of the quinary EMA with respect to those of the ternary alloy.

CONCLUSIONS

1. The oxidation behavior of three FeCoNi-base equi-molar alloys in dry air followed the parabolic rate law over the temperature range of 800–1000°C although two- or three-stage kinetics were observed in some cases.
2. The oxidation rate constants increased with increasing temperatures. The oxidation rates of the FeCoNi ternary alloy can be reduced by the addition of chromium or of chromium and copper, the most significant reduction occurring for the quaternary EMA at 800°C by 3.07 orders of magnitude.
3. The scales formed on the EMAs were complex and strongly composition-dependent and consisted of an outer layer of CoO, an intermediate layer of Fe_3O_4, and an inner layer of $CoNiO_2$ and Fe_3O_4 for the ternary alloy. Internal FeO precipitates were also observed for the ternary alloy. The scales formed on the quaternary EMA consisted of an outer layer of Fe_3O_4 and $CoCr_2O_4$, an intermediate layer of $FeCr_2O_4$ and $NiCr_2O_4$, and an inner layer of Cr_2O_3. Finally, the scales formed on the quinary alloy consisted of an outer layer of CuO, an intermediate layer of CuO and Fe_3O_4, and an inner layer of Fe_3O_4, $FeCr_2O_4$, and $CuCrO_2$.
4. The formation of Cr_2O_3 on the quaternary alloy and possibly that of $CuCrO_2$ on the quinary alloy was responsible for the reduction of oxidation rates, as compared to those of the ternary alloy.

ACKNOWLEDGMENTS

The authors would like to thank for the National Council of Republic of China for partly financial support under the Grant Nos. NSC 92-2216-E-019-005 and NSC 92-2216-E-019-008.

REFERENCES

1. F. H. Stott, G. C. Wood, and M. G. Hobby, *Oxidation of Metals* **3**, 103 (1971).
2. G. C. Wood and F. H. Stott, in *High Temperature Corrosion*, R. A. Rapp, ed., NACE, Houston, TX, USA, 1983.
3. S. Mrowec and K. Przybylski, *Oxidation of Metals* **23**, 107 (1985).
4. G. C. Wood and F. H. Stott, *Materials Science and Technology* **3**, 519 (1987).
5. H. Hindam and D. P. Whittle, *Oxidation of Metals* **18**, 245 (1982).
6. R. B. Schwarz and W. L. Johnson, *Physics Review Letters* **51**, 415 (1983).
7. A. Inoue and T. Zhang, *Materials Transactions JIM* **37**, 185 (1996).
8. W. Kai and R. T. Huang, *Oxidation of Metals* **48**, 439 (1997).
9. M. Takiguch, S. Ishii, E. Makino, and A. Okabe, *Journal of Applied Physics* **87**, 2469 (2000).

10. C. D. Liu, W. Kai, and Y. H. Shieh, *Journal of Chinese Corrosion Engineering* **14**, 45 (2000) (in Chinese).
11. P. Kofstad, *High Temperature Corrosion* (Elsevier Applied Science, London, 1988).
12. Y. Niu, Y. S. Li, and F. Gesmundo, *Corrosion Science* **42**, 165 (2000).
13. S. Mrowec and K. Przybylski, *Oxidation of Metals* **11**, 383 (1977).
14. D. W. Bridges, J. P. Baur, and W. M. Farrel, Jr., *Journal of the Electrochemical Society* **103**, 619 (1956).
15. K. Fueki and J. B. Wagner, Jr., *Journal of the Electrochemical Society* **112**, 384 (1965).
16. P. Kofstad, *Nonstoichiometry, Diffusion, and Electrical Conductivity in Binary Metals Oxides* (Robert E. Krieger Publishing Company, Florida, USA, 1983).
17. P. Vallet and P. Raccah, *Mem. Sci. Rev. Met*. **62**, 1 (1965).
18. B. Fisher and D. S. Tannhauser, *Journal of Chemical Physics* **44**, 1663 (1966).
19. Y. D. Tretyakov and R. A. Rapp, *Transactions AIME* **245**, 1235 (1969).
20. R. A. Rapp, *Corrosion* **21**, 382 (1965).
21. *Thermodynamic Data for Pure Substance*, 3rd edn. (American Chemical Society and American Institute of Physics for National Bureau of Standards, 1995).